inorganics

MDPI

Article

Mesoporous C/CrN and C/VN Nanocomposites Obtained by One-Pot Soft-Templating Process

Julien Kiener [1], Ovidiu Ersen [2,†] and Julien Parmentier [1,*,†]

[1] Université de Strasbourg, Université de Haute-Alsace, Institut de Science des Matériaux de Mulhouse—IS2M—UMR CNRS 7361, 15 rue Jean Starcky—BP 2488, Mulhouse Cedex 68057, France; julien.kiener@yahoo.com

[2] Institut de Physique et Chimie des Matériaux de Strasbourg, UMR 7504 CNRS—Université de Strasbourg, 23 rue du Loess, BP 43, Strasbourg Cedex 2 67034, France; ovidiu.ersen@ipcms.unistra.fr

* Correspondence: julien.parmentier@univ-mulhouse.fr; Tel.: +33-3-8960-8702; Fax: +33-3-8960-8789

† These authors contributed equally to this work.

Academic Editors: Samuel Bernard, André Ayral, Philippe Miele and Duncan H. Gregory

Received: 28 February 2016; Accepted: 30 June 2016; Published: 15 July 2016

Abstract: Nanocomposites of ordered mesoporous carbon associated with chromium nitride (CrN) or vanadium nitride (VN) nanoparticles were obtained by a simple one-pot synthesis based on the solvent evaporation induced self-assembly (EISA) process using Pluronic triblock surfactant as soft-template and a phenol-based resin (resol) as carbon precursor. These nanocomposites were characterized by X-ray diffraction, nitrogen physisorption and Transmission Electron Microscopy (TEM) techniques. Electron tomography (or 3D-TEM) technique was particularly useful for providing direct insight on the internal architecture of C/CrN nanocomposite. Nanocomposites showed a very well organized hexagonal mesoporous carbon structure and a relatively high concentration of nanoparticles well distributed in the porous network. The chromium and vanadium nitrides/mesoporous carbon nanocomposites could have many potential applications in catalysis, Li-ion batteries, and supercapacitors.

Keywords: mesopores; soft-template; one-pot; CrN; VN; nitride; Evaporation Induced Self-Assembly (EISA); nanocomposite; hybrid material; electron tomography

1. Introduction

Transition metal nitrides (TMN) are very promising materials for various applications such as hard coating, catalysis, energy storage (Li-based batteries and supercapacitors) and solar cells. As electrode material for Li-ion batteries, chromium nitride (CrN) and vanadium nitride (VN) may reach very large capacities after the first reduction step (1800 $mA \cdot h \cdot g^{-1}$ and 1500 $mA \cdot h \cdot g^{-1}$ respectively) [1], whereas CrN can maintain a relatively stable capacity upon cycling of 1200 $A \cdot h \cdot g^{-1}$ [2]. Other TMN have also been tested for application in Li-based batteries [3–6] and for various hydrotreating catalysis applications [7]. VN has been envisaged as a supercapacitor material [8–12] and has been tested as an oxygen reduction reaction (ORR) catalyst [13].

The performance of those materials can be further improved when they are present as nanoparticles and dispersed on an adequate support or inserted in a matrix. For the energy storage applications in Li-ion batteries for instance, the presence of dispersed nanoparticles promotes charge transfers of electrons or lithium ions [14] and extends the electrode lifespan [15] by limiting the volume variations of the electrode during lithium insertion/extraction cycles. The dispersion of these nanoparticles is achieved by using an adequate media that can provide other interesting functionalities such as high surface specific area, porosity (confinement) and electrical conductivity. In this general framework, the combination of TMN nanoparticles with porous carbon supports fills

all these requirements being thus potential materials for electrode materials in energy storage and electrocatalysis applications. Porous carbon matrix allows a good dispersion of TMN nanoparticles, limits their aggregation or their excessive growth (confinement in the porosity), ensures nanoparticles accessibility, provides good electric conductivity and can also be electrochemically active (ability of lithium intercalation/extraction in Li-ion batteries or double-layer capacitance for supercapacitors). For instance, the combination of vanadium nitride with carbon nanotubes in supercapacitor electrodes allows combining the strong pseudo-capacitance of VN with the good electronic conductivity of carbon nanotubes [9].

Direct synthesis of such nanocomposites combining TMN nanoparticles with porous carbon has rarely been investigated in the literature, especially using ordered mesoporous carbon as a dispersing media. This synthesis is based on the use of surfactant as soft-template and phenolic resin as carbon precursor. Their self-assembly leads to an organic polymeric ordered mesophase that is further converted to ordered mesoporous carbon by calcination in inert atmosphere [16,17]. The addition of a transition metallic salt in the first step of the preparation (one-pot synthesis) yields to a TM oxide/C nanocomposite that can be further converted to TMN/C by heat-treatment in NH_3 gas (ammonolysis). This route is easy and fast for obtaining such nanocomposites compared to other routes based on hard-template that are time consuming. To our knowledge, only titanium nitride/ordered mesoporous carbon has been prepared by this way in the literature [18,19]. The aim of this study is to demonstrate the versatility of the one-pot soft-template synthesis for the preparation of other TMN/C such as CrN/mesoporous C and VN/mesoporous C materials of particular interest for many potential applications. These materials were characterized by XRD, N_2 physisorption (77K), TEM and 3D TEM. Insights regarding their structures (e.g., nature of crystalline phases, nanoparticles size and distribution within the mesoporosity, and carbon mesostructuration degree) are discussed.

2. Results and Discussion

2.1. X-ray Diffraction (XRD) Characterization

XRD studies (Figure 1A) on FDU-15/CrN samples showed in the case of a nitridation temperature of 700 °C a poorly resolved pattern with three very large peaks that correspond to chromium nitride phase CrN. By increasing the nitridation temperature, several XRD peaks, thinner and more intense than before, were clearly observed owing to the CrN nanoparticles growth. At 950 °C, CrN crystallization degree is sufficient to be able to calculate accurately its cubic lattice parameter (4.143 ± 0.004 Å); the value is in good agreement with that reported in the literature (4.140 Å) [20]. At 850 °C, a secondary phase of chromium carbonitride phase appeared ($Cr_{6.2}C_{3.5}N_{0.3}$) due to the reaction between the Cr-based phase and the carbon matrix. This reaction continued at 950 °C, where a more crystallized $Cr_{6.2}C_{3.5}N_{0.3}$ phase appeared together with the pure chromium carbide phase (Cr_3C_2). The XRD studies on FDU-15/CrN nanocomposites showed that these samples followed the same trend as the TiO_2/C nanocomposites [19,21], i.e., the formation of a nitride phase between 700 and 800 °C followed at higher temperature by that of a carbide phase.

A different behavior was observed for the FDU15/VN samples during the nitriding step (Figure 1B). Owing to the fact that vanadium monoxide VO (ICDD 00-010-0313) and vanadium nitride VN (ICDD 00-035-0768) have the same crystal structure (face-centered cubic *Fm-3m*) and close lattice parameters (4.093 Å for VO and 4.139 Å for VN), the phase assignment could rely only on a very accurate cell parameter determination. However, as the XRD patterns were poorly resolved for the nitridation temperatures of 750 and 850 °C, it was difficult to differentiate between VO and VN phases. At 950 °C, the peaks become more thin and intense and allowed a precise lattice parameter determination (4.136 ± 0.006 Å). By applying the linear Vegard's law, this phase corresponds to a partially nitrided phase with composition ranging from $VO_{0.2}N_{0.8}$ to VN. Vanadium carbide phase was not considered here as potentially present owing to its higher cell-parameter (4.17 Å) comparing to VN.

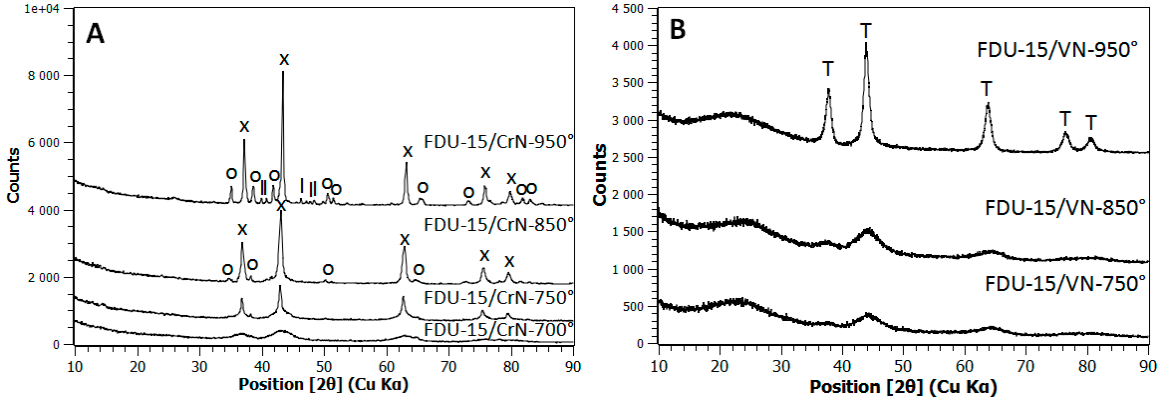

Figure 1. XRD diagrams for FDU-15/CrN (**A**) and FDU-15/VN (**B**) samples. Symbols are: x for CrN (ICDD 00-011-0065), o for $Cr_{6.2}C_{3.5}N_{0.3}$ (ICDD 00-019-0065), l for Cr_3C_2 (ICDD 00-035-0804) and T for VN (ICDD 00-035-0768).

2.2. Nitrogen Adsorption Measurements (77K)

All isotherms presented in Figure 2 are characterized by type I and type IV components, having high adsorption capacity at low pressure and hysteresis loops, respectively. These two types of porosity can be observed on the pore size distribution given in Figure 3. Mesopores have a diameter relatively well defined, around 4.5 nm. All the porous characteristics of these materials are summarized in Table 1, together with the data obtained for pure FDU-15 carbon materials prepared in argon or ammonia at 850 °C used as reference samples and denoted FDU-15-850°-Ar and FDU-15-850°-NH_3 respectively. Comparison of both FDU-15 carbon references showed clearly the influence of the high-temperature ammonia treatment on the activation of the porosity in the microporous range (micropore volume increased from 0.11 to 0.18 cm^3/g) without modifying the mesopore volume. This phenomena was already reported in the literature [22]. The influence of the temperature used for the ammonia treatment is difficult to explain since antagonist phenomena could occur with the increase of the temperature: the formation of the micropores related to the presence of some volatile chemical species during the carbonization (CO, CO_2, and H_2O) and the activation step by ammonia, the collapse and/or shrinkage of the porous structure during the treatments, the reaction between the carbon matrix and the TM-based nanoparticles (carbothermal reduction, carbidation and/or carbonitridation).

When TM salts have been introduced in the synthesis media, porous features slightly decrease compared to the FDU-15 carbon reference treated in NH_3 (FDU-15-850°-NH_3) owing to the high density of the TMN part. By subtracting the TMN part (21 wt % for CrN and 28 wt % for VN in C/TMN nanocomposites), the contribution of the carbon part could be estimated for composite materials prepared at the same temperature as the reference material (FDU-15/CrN-850° and FDU-15/VN-850° samples). It appears that specific surface areas, and micropore and mesopore volumes of the carbon matrices increased compared to pure FDU-15 carbon treated in NH_3 at the same temperature (850 °C). This can be observed by comparing the values in Table 1 for the FDU-15-850°-NH_3 sample (e.g., specific surface area 524 m^3/g) with those in brackets corresponding to the FDU-15/CrN-850° and FDU-15/VN-850° samples (e.g., 983 and 1101 m^2/g, respectively). This feature could be related either to a modification of the carbon mesostructuration during the EISA process and/or a porosity activation process related to the presence of TM [23,24]. It also suggests that no significant pore blocking, owing to the presence of TMN nanoparticles in the carbon matrix occurs since all the porosity seems to be accessible to N_2 probe.

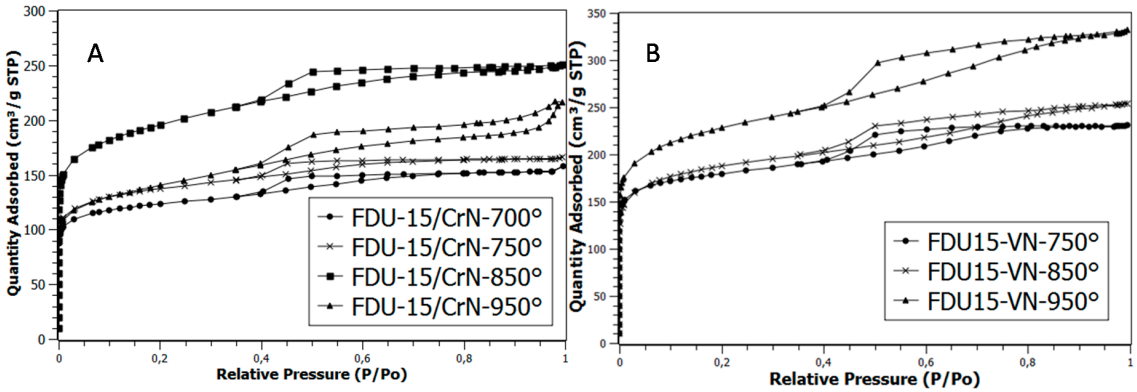

Figure 2. N_2 adsorption isotherms at 77 K for the FDU-15/CrN (**A**) and FDU-15/VN (**B**) mesoporous samples.

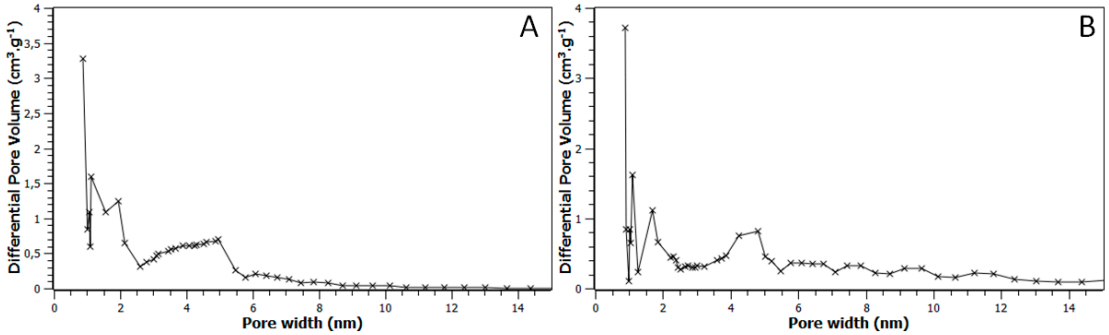

Figure 3. Pore size distribution for the FDU-15/CrN-850° (**A**) and FDU-15/VN-950° (**B**) mesoporous specimens. Note that these distributions have been obtained using the DFT method and assuming a cylindrical pore model.

Table 1. Quantitative results of N_2 physisorption measurements at 77 K.

Samples	S_{DFT} ($m^2 \cdot g^{-1}$) *	$V_{total\ pores}$ ($cm^3 \cdot g^{-1}$) *	$V_{micropores}$ ($cm^3 \cdot g^{-1}$) *	$V_{mesopores}$ ($cm^3 \cdot g^{-1}$) *
FDU-15-850°-Ar	344	0.29	0.11	0.18
FDU-15-850°-NH_3	524	0.36	0.18	0.18
FDU-15/CrN-700°	660	0.22	0.15	0.07
FDU-15/CrN-750°	357	0.16	0.09	0.07
FDU-15/CrN-850°	777 (983)	0.33 (0.42)	0.16 (0.20)	0.17 (0.22)
FDU-15/CrN-950°	709	0.28	0.14	0.14
FDU-15/VN-750°	1046	0.35	0.23	0.12
FDU-15/VN-850°	870 (1101)	0.35 (0.44)	0.18 (0.23)	0.17 (0.21)
FDU-15/VN-950°	1154	0.49	0.22	0.27

* These values have been calculated with DFT method by assuming a cylindrical pore model. Values given in bracket correspond to the individual carbon phase contributions by subtracting transition metal nitride (TMN) contributions (see details in supplementary materials, thermogravimetric analysis). These TMN weight contributions, calculated from TGA (see Figures S1 and S2 in supplementary materials), were equal to 21 wt % for C/CrN and 28 wt % for C/VN nanocomposites.

2.3. TEM Results

General morphological and structural characteristics of these nanocomposites have been obtained by classical TEM, while a more detailed study by electron tomography (3D-TEM) has been realized on one of the specimens of interest, i.e., FDU-15/CrN-850°.

The analysis of the FDU-15/CrN-850° specimen by classical TEM (Figure 4) showed a very well organized mesoporous carbon matrix (hexagonal cell parameter equal to 17 nm) and a relatively high amount of CrN nanoparticles well dispersed in the matrix. The nanoparticles diameters are between 5

and 20 nm. A crucial piece of information is that the high organization degree of the carbon matrix at the mesoscopic scale (mesoporosity) can be maintained even for a high concentration of nanoparticles (>20 wt %). Few aggregates with a diameter between 100 and 200 nm can also be observed in some specific regions (data not shown).

The classical TEM observations performed on the FDU-15/VN-950° sample (Figure 5) also showed a very well organized mesoporous carbon matrix (hexagonal cell parameter equal to 18 nm) that contains a high density of VN nanoparticles very well dispersed as well. However, in this case, the mean size distribution of nanoparticles is larger (between 5 and 40 nm), which could be explained by a lower dissolution of the vanadium precursor in ethanol compared to that of the chromium precursor. Few aggregates (with a diameter larger than 100 nm) were also observed.

For both samples, the average diameter of TMN nanoparticles was similar or slightly higher than the diameter of mesopores (Figure S3). Smaller particles seem to be located in the mesopores whereas bigger ones also are present within the carbon wall. These phenomena are frequently encountered with the one-pot synthesis of ordered mesoporous carbon embedding metal-based nanoparticles [25]. Though the use of soluble precursors and the presence of carbon matrix are supposed to disperse (and dilute) the transition metal to limit their sintering during heat-treatment, it cannot inhibit sufficiently the TM segregation and nanoparticles growth above the size of the mesopores. Electron tomography (3D-TEM) was used to get more insight regarding the location of the TMN nanoparticles and the structuration of the carbon matrix around these nanoparticles in the TMN/C composites.

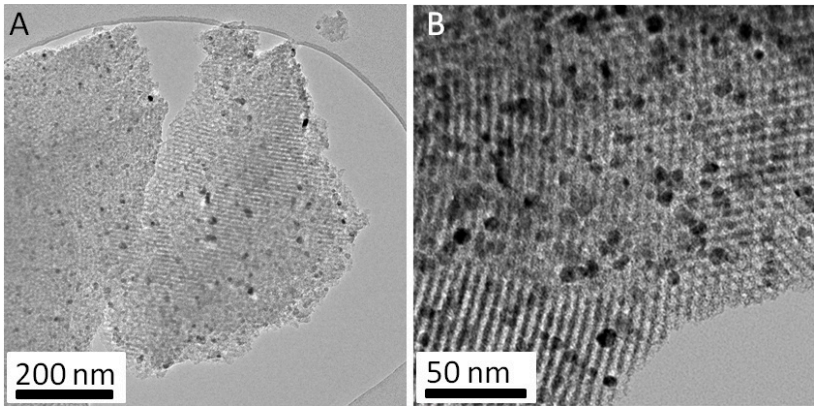

Figure 4. Classical TEM images for the FDU-15/CrN-850° sample at lower (**A**) and higher (**B**) magnification.

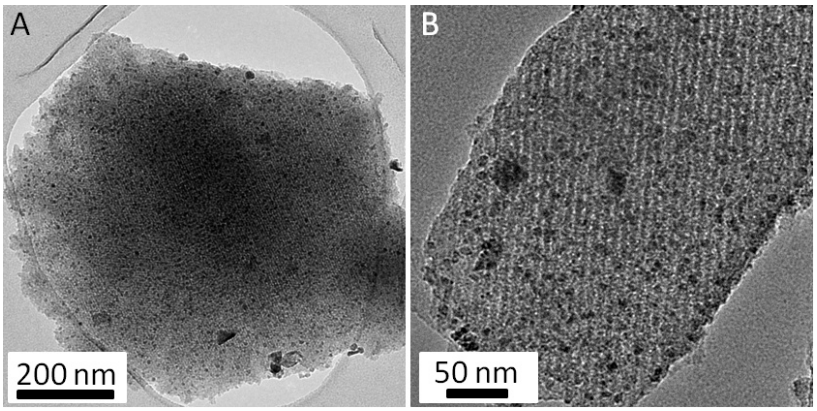

Figure 5. Typical TEM micrographs acquired on the FDU-15/VN-950° sample at lower (**A**) and higher (**B**) magnification.

Electron tomography (3D-TEM) is a 3D imaging mode with nanometer resolution that allows reconstructing in three dimensions the volume of an object, whereas classical TEM images provide only its 2D projections. In our case, this technique provided crucial information on the internal structure of the nanocomposites, more precisely on the spatial distribution of the nanoparticles. Typical electron tomography slices along and perpendicularly to the main axis of the hexagonal FDU-15/CrN-850° matrix are shown in Figure 6. By analyzing the transversal slices, the hexagonal symmetry of the porous network can be easily observed and its cell parameter determined (17 nm). These slices showed that nanoparticles were well located inside the mesoporous network, more precisely in the mesopores, and not on the external surface (Figure 6A). For large TMN particles (size from 5 up to 200 nm), with a size larger than the mesopore diameter, 3D-TEM slices also confirmed their location in the carbon matrix (Figure 7). However, the carbon mesoporous structure seems to be slightly distorted around the particles, illustrating that their growth led to a partial loss of the hexagonal mesopore array in their vicinity. Those nanoparticles appeared also surrounded by small partial voids (free space) in the matrix that could be related to the modifications of the mesoperiodicity around the nanoparticles and/or to the carbon consumption for the formation of carbide phase ($Cr_{6.2}C_{3.5}N_{0.3}$). In all cases, based on the combined analysis by 3D-TEM and N_2 physisorption data, small and big particles seem to remain accessible to fluids, which is a very important requirement for potential applications as catalysis and supercapacitor.

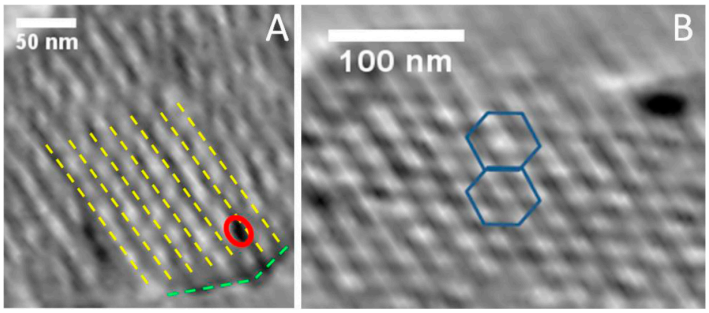

Figure 6. Longitudinal (**A**) and transversal (**B**) 3D-TEM slices for the FDU-15/CrN sample. Yellow lines correspond to the pores walls, whereas the red circle delimitates a nanoparticle. The green lines schematize the surface of the analyzed mesoporous grain. On the transversal slice (**B**), the hexagonal symmetry of the porous structure can be clearly evidenced.

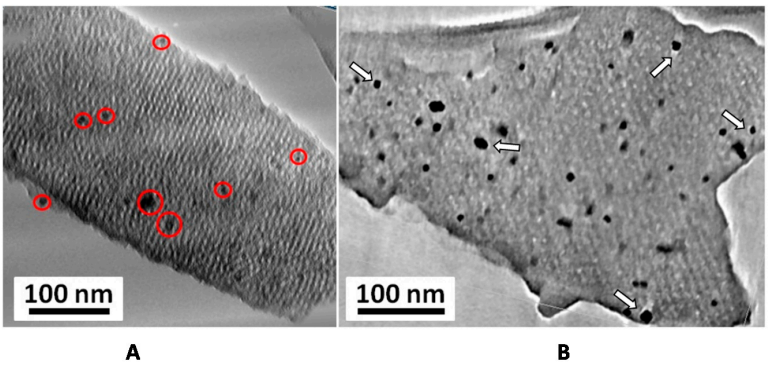

Figure 7. Typical TEM-3D slices extracted from the reconstructed volumes obtained for the FDU-15/CrN-850° sample showing the presence of TMN nanoparticles with a size larger than the mesopores diameter. These nanoparticles (highlighted by red circles in (**A**)) are embedded in the ordered mesoporous carbon matrix. Arrows (**B**) indicate the presence of voids (porosity) around these big particles. The smaller nanoparticles are not visible here due to the low magnification of the chosen slices presented on this figure.

3. Experimental Section

Synthesis of mesoporous C/CrN and C/VN nanocomposites were based on the evaporation-induced self-assembly process (EISA) and derived from the procedure developed by Meng et al. [17] for the mesoporous carbon phase denoted FDU-15. First, the carbon precursor was prepared by mixing phenol (0.61 g) with formaldehyde (1.06 g of 37 wt % formaldehyde solution) in basic media (0.13 g of NaOH aqueous solution at 20 wt %). The mixture was further heated to 71 °C for 60 min for allowing the polycondensation of phenol to a prepolymer named resol. After cooling to room temperature, the pH value of the solution was adjusted to neutral by using dilute HCl solution (0.6 M). The resol was dried at 48 °C in a vacuum rotary evaporator to remove water and then was solubilized in 9.6 g of ethanol (solution A).

Simultaneously, Pluronic F127 (1.0 g), a triblock copolymer of average formula $HO(CH_2CH_2O)_{100}(CH_2CH(CH_3)O)_{65}(CH_2CH_2O)_{100}H$ and either chromium nitrate nonahydrate (0.5 g) or vanadium acetylacetonate (1.0 g) were dissolved in 9.6 g of ethanol (solution B). Solution A was poured into solution B. This mixture was then stirred for 1 h before to be deposed in thin films (1 mm thickness) in Petri dishes, dried at room temperature for 12 h and afterward heated at 100 °C for 24 h. During this drying step, an evaporation induced self-assembly process took place with formation of tubular micelles of Pluronic F127 associated with resol in their hydrophilic external shells. Those composite micelles formed a mesophase having a hexagonal symmetry (space group *P6mm*). The resulting dried films were scratched and calcined in a tubular furnace under argon (flow 9 $L \cdot h^{-1}$) up to the desired temperature. This heat-treatment led to the carbonization of the phenolic resin to carbon, whereas the Pluronic, being the porogen agent, was decomposed to gaseous species and released the ordered porosity of the material. Then, the nitriding treatment was performed for 3 h in ammonia (4 $L \cdot h^{-1}$) at the same temperature to convert the transition metal oxide to nitride. The heating ramps were 1 °C/min from room temperature to 600 °C and 5 °C/min from 600 °C to the final temperature. All chemicals were purchased from Sigma-Aldrich Inc. (Saint-Quentin Fallavier, France). Samples were labeled as follows: FDU-15/VN-X or FDU-15/CrN-X, where X corresponds to the temperature used for the nitriding step (°C). Pure FDU-15 carbon materials prepared in argon or ammonia (850 °C) were used as references. Nitrogen adsorption isotherms were measured at 77 K using an ASAP 2420 (Micromeritics, Norcross, GA, USA). Samples were outgased at 200 °C overnight before measurements. Surface areas, pore size distributions and pore volumes were obtained by the DFT method using Micromeritics 2420 software considering a cylindrical pore shape. X-ray Diffraction (XRD) measurements were recorded on a X'Pert MPD (Panalytical, Lelyweg, The Netherlands) with Cu Kα radiation (1.54 Å). Cell parameters were determined using the free software Eracel (IUCr, http://www.cristal.org/ftp/eracel.zip). TGA curves are presented in the supplementary materials (Figures S1 and S2). From this technique, weight percent for chromium nitride and vanadium nitride in both nanocomposites were estimated as 21 wt % and 28 wt %, respectively. For the conventional TEM analyses, a CM200 (Philips, Amsterdam, The Netherlands) was used. A JEOL 2100F TEM (JEOL USA, Inc., Pleasanton, CA, USA) operating at 200 kV was used for high resolution microscopy and for electron tomography. The tilt series were recorded automatically using the GATAN tomography software (Gatan Inc., Pleasanton, CA, USA), within the angular range spanning from −75° to +75° with an increment of 1.5°. The fine alignment of the tilt series and the volume reconstructions were performed by using the IMOD software (University of Colorado, Boulder, CO, USA).

4. Conclusions

We have demonstrated the possibility to obtain mesoporous C/VN and C/CrN nanocomposites by a simple one-pot soft-template synthesis. They are constituted by an ordered mesoporous carbon matrix, which embeds a relatively high amount of TMN nanoparticles (around 20 wt %) well dispersed within the carbon matrix. The presence of the metal modifies the EISA and/or ammonia heat-treatment (850 °C) processes leading to an increase of the pore volumes (micro and meso) and of the surface area of the carbon part, which suggests the absence of pore blocking by nanoparticles. Electron

tomography study showed that the nanoparticles are clearly located inside the carbon matrix: (i) in the mesopores for the small nanoparticles (around 5 nm in diameter); and (ii) embedded in the porous carbon framework for those exceeding that diameter (particle size from 5 up to 200 nm), thus leading to, locally around particles, a slightly disordered mesostructure with small additional partial voids (free space). For both particles sizes, their surface accessibility to fluid seems ensured, which is a very important requirement for the potential applications of these composites in catalysis or energy storage.

Supplementary Materials: The following are available online at www.mdpi.com/2304-6740/4/3/22/s1, Figure S1: TGA curves of FDU-15/CrN-850°. Figure S2: TGA curves of FDU-15/VN-950°. Figure S3: TEM picture at high magnification and TMN particle size distribution of FDU-15/CrN-850° (**A**) and FDU-15/VN-950° (**B**).

Author Contributions: Main experimental work and writing of the manuscript were done by Julien Kiener. Supervision of these tasks was performed by Ovidiu Ersen and Julien Parmentier.

Conflicts of Interest: The authors declare no conflict of interest.

References

1. Cabana, J.; Monconduit, L.; Larcher, D.; Palacín, M.R. Beyond Intercalation-Based Li-Ion Batteries: The State of the Art and Challenges of Electrode Materials Reacting Through Conversion Reactions. *Adv. Mater.* **2010**, *22*, E170–E192. [CrossRef] [PubMed]
2. Sun, Q.; Fu, Z.-W. An Anode Material of CrN for Lithium-Ion Batteries. *Electrochem. Solid State Lett.* **2007**, *10*, A189–A193. [CrossRef]
3. Das, B.; Reddy, M.V.; Malar, P.; Osipowicz, T.; Subba Rao, G.V.; Chowdari, B.V.R. Nanoflake CoN as a high capacity anode for Li-ion batteries. *Solid State Ion.* **2009**, *180*, 1061–1068. [CrossRef]
4. Wang, Y.; Liu, W.Y.; Fu, Z.-W. Electrochemistry of Mn4N with Lithium. *Acta Phys. Chim. Sin.* **2006**, *22*, 65–70.
5. Wang, Y.; Fu, Z.-W.; Yue, X.-L.; Qin, Q.-Z. Electrochemical Reactivity Mechanism of Ni_3N with Lithium. *J. Electrochem. Soc.* **2004**, *151*, E162–E167. [CrossRef]
6. Fu, Z.-W.; Wang, Y.; Yue, X.-L.; Zhao, S.-L.; Qin, Q.-Z. Electrochemical Reactions of Lithium with Transition Metal Nitride Electrodes. *J. Phys. Chem. B* **2004**, *108*, 2236–2244. [CrossRef]
7. Nagai, M. Transition-metal nitrides for hydrotreating catalyst—Synthesis, surface properties, and reactivities. *Appl. Catal. A Genet.* **2007**, *322*, 178–190. [CrossRef]
8. Choi, D.; Blomgren, G.E.; Kumta, P.N. Fast and Reversible Surface Redox Reaction in Nanocrystalline Vanadium Nitride Supercapacitors. *Adv. Mater.* **2006**, *18*, 1178–1182. [CrossRef]
9. Ghimbeu, C.M.; Raymundo-Piñero, E.; Fioux, P.; Béguin, F.; Vix-Guterl, C. Vanadium nitride/carbon nanotube nanocomposites as electrodes for supercapacitors. *J. Mater. Chem.* **2011**, *21*, 13268. [CrossRef]
10. Lu, X.; Yu, M.; Zhai, T.; Wang, G.; Xie, S.; Liu, T.; Liang, C.; Tong, Y.; Li, Y. High Energy Density Asymmetric Quasi-Solid-State Supercapacitor Based on Porous Vanadium Nitride Nanowire Anode. *Nano Lett.* **2013**, *13*, 2628–2633. [CrossRef] [PubMed]
11. Simon, P.; Gogotsi, Y. Materials for electrochemical capacitors. *Nat. Mater.* **2008**, *7*, 845–854. [CrossRef] [PubMed]
12. Zhou, X.; Chen, H.; Shu, D.; He, C.; Nan, J. Study on the electrochemical behavior of vanadium nitride as a promising supercapacitor material. *J. Phys. Chem. Solids* **2009**, *70*, 495–500. [CrossRef]
13. Huang, T.; Mao, S.; Zhou, G.; Wen, Z.; Huang, X.; Ci, S.; Chen, J. Hydrothermal synthesis of vanadium nitride and modulation of its catalytic performance for oxygen reduction reaction. *Nanoscale* **2014**, *6*, 9608. [CrossRef] [PubMed]
14. Zhang, Q.; Uchaker, E.; Candelaria, S.L.; Cao, G. Nanomaterials for energy conversion and storage. *Chem. Soc. Rev.* **2013**, *42*, 3127. [CrossRef] [PubMed]
15. Yin, Y.-X.; Xin, S.; Guo, Y.-G. Nanoparticles Engineering for Lithium-Ion Batteries. *Part. Part. Syst. Charact.* **2013**, *30*, 737–753. [CrossRef]
16. Zhang, F.; Meng, Y.; Gu, D.; Yan; Yu, C.; Tu, B.; Zhao, D. A Facile Aqueous Route to Synthesize Highly Ordered Mesoporous Polymers and Carbon Frameworks with $Ia\bar{3}d$ Bicontinuous Cubic Structure. *J. Am. Chem. Soc.* **2005**, *127*, 13508–13509. [CrossRef] [PubMed]

17. Meng, Y.; Gu, D.; Zhang, F.; Shi, Y.; Yang, H.; Li, Z.; Yu, C.; Tu, B.; Zhao, D. Ordered Mesoporous Polymers and Homologous Carbon Frameworks: Amphiphilic Surfactant Templating and Direct Transformation. *Angew. Chem.* **2005**, *117*, 7215–7221. [CrossRef]
18. Ramasamy, E.; Jo, C.; Anthonysamy, A.; Jeong, I.; Kim, J.K.; Lee, J. Soft-Template Simple Synthesis of Ordered Mesoporous Titanium Nitride-Carbon Nanocomposite for High Performance Dye-Sensitized Solar Cell Counter Electrodes. *Chem. Mater.* **2012**, *24*, 1575–1582. [CrossRef]
19. Schlienger, S.; Ersen, O.; Roiban, L.; Parmentier, J. Direct Synthesis of TiN/Mesoporous Carbon Nanocomposite by Nitridation of a Hybrid Inorganic/Organic Mesostructured Material. *J. Am. Ceram. Soc.* **2011**, *94*, 4142–4145. [CrossRef]
20. Buchwald, V.F.; Scott, E.R.D. First Nitride (CrN) in Iron Meteorites. *Nat. Phys. Sci.* **1971**, *233*, 113–114. [CrossRef]
21. Huang, C.-H.; Gu, D.; Zhao, D.; Doong, R.-A. Direct Synthesis of Controllable Microstructures of Thermally Stable and Ordered Mesoporous Crystalline Titanium Oxides and Carbide/Carbon Composites. *Chem. Mater.* **2010**, *22*, 1760–1767. [CrossRef]
22. Mangun, C.L.; Benak, K.R.; Economy, J.; Foster, K.L. Surface chemistry, pore sizes and adsorption properties of activated carbon fibers and precursors treated with ammonia. *Carbon* **2001**, *39*, 1809–1820. [CrossRef]
23. Maldonado-Hódar, F. Surface morphology, metal dispersion, and pore texture of transition metal-doped monolithic carbon aerogels and steam-activated derivatives. *Microporous Mesoporous Mater.* **2004**, *69*, 119–125. [CrossRef]
24. Maldonado-Hódar, F.J.; Moreno-Castilla, C.; Rivera-Utrilla, J.; Hanzawa, Y.; Yamada, Y. Catalytic Graphitization of Carbon Aerogels by Transition Metals. *Langmuir* **2000**, *16*, 4367–4373. [CrossRef]
25. Matei Ghimbeu, C.; Puscasu, A.; Martinez de Yuso, A.; Zlotea, C.; Oumellal, Y.; Latroche, M.; Vix-Guterl, C. One-pot synthesis of tailored Pd–Co nanoalloy particles confined in mesoporous carbon. *Microporous Mesoporous Mater.* **2016**, *223*, 79–88. [CrossRef]